PROCEEDINGS OF SPIE

SPIEDigitalLibrary.org/conference-proceedings-of-spie

Enhanced resolution dispersion optimized multiphoton microscopy with spatial frequency modulation imaging

Daniel Scarbrough, Anna Thomas, Jeff Field, Randy Bartels, Jeff Squier

Daniel Scarbrough, Anna Thomas, Jeff Field, Randy Bartels, Jeff Squier, "Enhanced resolution dispersion optimized multiphoton microscopy with spatial frequency modulation imaging," Proc. SPIE 12384, Multiphoton Microscopy in the Biomedical Sciences XXIII, 123840O (25 April 2023); doi: 10.1117/12.2650490



Event: SPIE BiOS, 2023, San Francisco, California, United States

Enhanced Resolution Dispersion Optimized Multiphoton Microscopy with Spatial Frequency Modulation Imaging

Daniel Scarbrough^a, Anna Thomas^a, Jeff Field^{b,c}, Randy Bartels^{b,d}, and Jeff Squier^a

^aColorado School of Mines Department of Physics, 1500 Illinois St, Golden, CO, USA ^bDepartment of Electrical and Computer Engineering, Colorado State University, Fort Collins, Colorado 80523, USA

^cCenter for Imaging and Surface Science, Colorado State University, Fort Collins, Colorado 80523, USA

^dSchool of Biomedical Engineering, Colorado State University, Fort Collins, Colorado 80523, USA

ABSTRACT

Using the structured illumination, single pixel detection imaging technique SPatIal Frequency modulation Imaging (SPIFI), we demonstrate a cascaded Wavelength Domain and Spatial Domain (WD-SD-SPIFI) system enabling real-time, in-line, second order dispersion compensation optimization for multiphoton imaging. Enhanced resolution is demonstrated by imaging a sub-diffractive 140 nm fluorescent nanodiamond with Two Photon Excitation Fluorescence (2PEF) to measure the Point Spread Function (PSF). With a 1034 nm pulsed laser through a Numerical Aperture (NA) of 0.5, a PSF Full Width at Half Max (FWHM) of 780 nm was measured with minimal post processing analysis that only requires Fast Fourier Transforms (FFTs).

Keywords: Microscopy, structured illumination, multiphoton, enhanced resolution, SPIFI, dispersion compensation, single pixel detection

1. INTRODUCTION

Structured Illumination Microscopy (SIM) covers a multitude of imaging techniques with the goal of providing a benefit or benefits over traditional microscopic imaging and confocal microscopy. Since its early conception by Köhler, SIM has taken many forms enabling enhanced resolution. The HiLo technique^{2,3} for example has been extended to Light Sheet Fluorescence Microscopy (LSFM), multiphoton temporal focusing, and line scanning. Other forms of SIM have been developed to achieve enhanced resolution using techniques such as interferometry, intensity modulation, fiber arrays, and temporal encoding. Recent computational advances have enabled deep learning to be applied to standard commercial SIM instruments to improve resolution. Common among these techniques is the use of high quality 2D array detectors (CCD, cMOS), or modulation devices such as Spatial Light Modulators (SLM) or Digital Micromirror Devices (DMD). These devices can significantly increase system cost, especially in comparison to systems that rely on single pixel detection or more cost-effective modulation schemes.

Single pixel detection pairs well with SIM as the structure enables multidimensional image reconstruction despite the zero dimensional detector. Compressive sensing with an L1 norm minimization has achieved 100 frames per second (fps), ¹² and others have gone to kHz rates using Acousto Optic Modulators (AOM). ¹³ Multiphoton compatible techniques have also been demonstrated using temporal focusing from a DMD, ¹⁴ and another technique uses a more cost effective spinning mask modulation for Hadamard reconstruction. ¹⁵ While single pixel SIM is demonstrated by these, enhanced resolution is not among the benefits.

One technique which takes advantage of both structured illumination and single element detection is SPatIal Frequency modulation Imaging (SPIFI). SPIFI encodes temporal frequency information onto the spatial domain

Further author information: (Send correspondence to Daniel Scarbrough)

Daniel Scarbrough: E-mail: dscarbro@mines.edu

Multiphoton Microscopy in the Biomedical Sciences XXIII, edited by Ammasi Periasamy, Peter T. C. So, Karsten König, Proc. of SPIE Vol. 12384, 1238400 © 2023 SPIE · 1605-7422 · doi: 10.1117/12.2650490

of a line cursor. Commonly this encoding is imparted via a rotating reticle on which a pattern based on the Lovell electro-optical position indicator¹⁶ is printed. This pattern has a frequency modulation that changes linearly with radius.¹⁷ As this modulation mask rotates each pixel along the line cursor is modulated at a unique temporal frequency. This mapping from the spatial domain to a temporal frequency domain enables single element detection by measuring the collected signal in time and reconstructing the image data with an FFT. This mitigates the effects of scattering following focus onto the sample which may be seen when imaging with a 2D detector array through a diffusive sample. Since SPIFI uses an FFT reconstruction it maintains a low reconstruction complexity of $O(M N \log N)$, where M is the number of line images and N is the number of points the FFT is performed on. Additionally with the line scanning inherent to SPIFI, pixel dwell time is improved over point rasterization techniques. For example a 256x256 pixel image taken at 30 fps with a point scanning technique has only 510 ns of exposure per pixel. For multiphoton imaging with a pulsed laser at a repetition rate of 100 MHz this would result in 50 pulses incident on each pixel. However for a line scanning architecture where the line is scanned across 256 steps, a 30 fps image can be taken with a pixel dwell time of 130 μ s and 13,020 pulses per pixel. Since SPIFI was first introduced as an imaging technique, ^{18–20} it has been demonstrated and extended to multiple applications including multiphoton imaging, ²¹ multi-cursor 2D imaging, ²² random access multiphoton imaging, ²³ and Coherent Anti-stokes Raman Spectroscopy (CARS). ²⁴

The SPIFI modulation mask is modeled in polar coordinates according to:

$$M(r, \theta(t)) = \frac{1}{2} (1 + \cos[k(r_0 + r)\theta(t)])$$
(1)

Where r is the radius on the mask and $\theta(t)$ is the rotation of the mask at one time step. The spatial frequency of the mask pattern at each angle is determined by the chirp rate k and the offset r_0 . At each position of r, a unique temporal frequency is encoded throughout the mask rotation. This encoding enables image reconstruction via an FFT of the time signal. Here we summarize the analysis of the SPIFI signals presented in 25 and account for second order multiphoton imaging as in Two-Photon Excitation Fluorescence (2PEF) or Second Harmonic Generation (SHG). For simplicity, the mask equation is written with a time dependent spatial frequency $f_r(t)$:

$$M(r,t) = \frac{1}{2} (1 + \cos[2\pi f_r(t)r])$$
 (2)

The mask modulates the electric field which is a line cursor along r, E(r). Following that the modulated field passes through the object c(r) resulting in E(r)M(r,t)c(r). The detector reads the intensity of this field so it is squared: E(r) becomes I(r), M(r,t) is simplified with a trigonometric reduction using the identity $\cos^2(\theta) = 1/2(1 + \cos(2\theta))$, and $c^2(r)$ is written as C(r) for simplicity. For a 2nd order process such as 2PEF, the intensity is squared for a two-photon dependent fluorescence intensity. For the object in two-photon (2P), it is written as $C_{2P}(r)$ to represent the two-photon spatial response.

$$I_m(r,t) = I(r) \frac{1}{8} \left(3 + 4\cos[2\pi f_r(t)r] + \cos[2\pi 2f_r(t)r] \right) C(r)$$
(3)

$$I_m^2(r,t) = I^2(r)\frac{1}{128}(35 + 56\cos[2\pi f_r(t)r] + 28\cos[2\pi 2f_r(t)r]$$
(4)

$$+8\cos[2\pi \, 3f_r(t)r] + \cos[2\pi \, 4f_r(t)r])C_{2P}(r) \tag{5}$$

Each of these terms in the intensity can be examined individually to analyze the detected signal. As the single element detector spatially integrates the full intensity signal we can look at the integral of each term independently. The leading constants and time dependent amplitude (due to modulation and vignetting) are wrapped into $H_q(t)$ where q represents the "order" of the term. Expanding these terms with the Euler integral as shown in Equations (6-9) results in a Fourier transform, and the factors of 1, 2, 3, and 4 on $f_r(t)$ are carried through onto the spatial frequency argument of the Fourier Transform of the object's 2P response. This indicates an increase in the spatial frequency support for imaging the object on increasing SPIFI orders q.

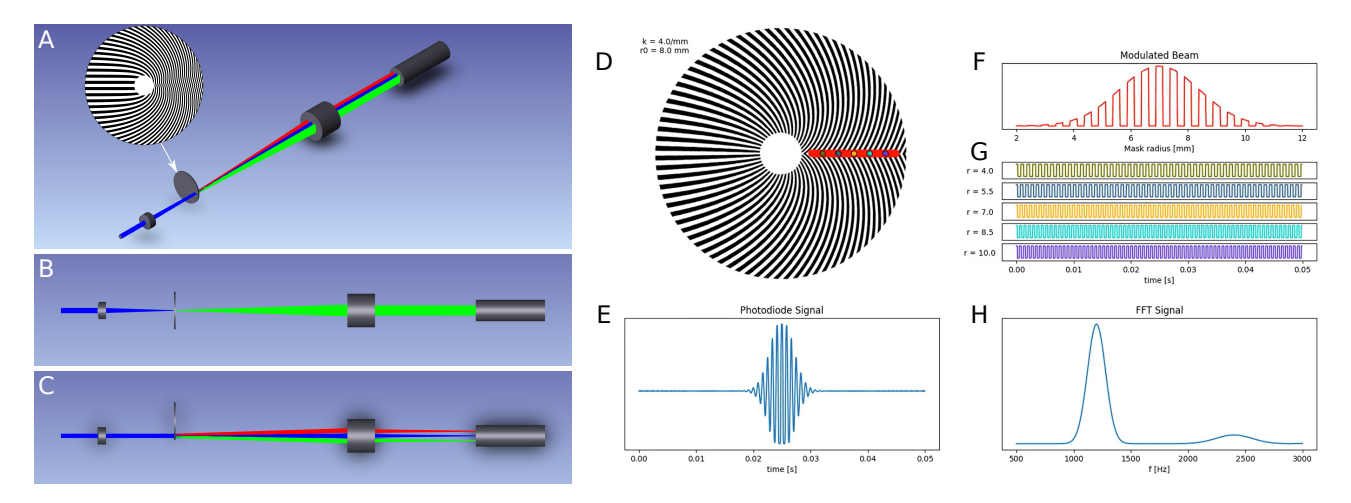


Figure 1. **A**: Isometric view of a SPIFI microscope. **B**: X-Z view of SPIFI microscope **C**: Y-Z view of SPIFI microscope. This view makes clear the line focus on the SPIFI mask, the diffracted orders from the SPIFI mask, and the spread of the diffracted orders on the objective pupil. **D**: Simulated SPIFI mask with parameters $k = 4.0 \text{ m m}^{-1}$ and $r_0 = 8.0$. The red line represents the focused line beam and the colored dots along it correspond to single pixels on the line whose modulations are shown in **G**. **E**: Simulated time signal from a photodiode. This is the spatial integral along the line cursor at each time step, corresponding to one rotation step. No object is present in this simulation. **F**: Intensity profile of the line cursor at one modulation time step. **G**: Normalized modulation of each colored pixel highlighted in **D**. Each pixel has a unique temporal frequency which enables its extraction into a line image via FFT. **H**: FFT of the SPIFI trace in **E** which shows the first and second order i mages. Note the second order is centered at twice the frequency of the first order, the amplitude is lower, and the width of the second order is twice that of the first. **Video 1**: Sections **D-H** of this figure are featured from a full SPIFI simulation which can be found at http://dx.doi.org/10.1117/12.2650490.1

$$S_{\pm 1}(t) = H_1(t) \int_{\infty}^{\infty} dr \, \exp(\pm i \, 2\pi \, f_r(t) r) C_{2P}(r) = H_1(t) \tilde{C}_{2P}(\pm f_r(t))$$
 (6)

$$S_{\pm 2}(t) = H_2(t) \int_{-\infty}^{\infty} dr \, \exp(\pm i \, 2\pi \, 2 \, f_r(t) r) C_{2P}(r) = H_2(t) \tilde{C}_{2P}(\pm 2 \, f_r(t))$$
 (7)

$$S_{\pm 2}(t) = H_3(t) \int_{-\infty}^{\infty} dr \, \exp(\pm i \, 2\pi \, 3 \, f_r(t) r) C_{2P}(r) = H_3(t) \tilde{C}_{2P}(\pm 3 \, f_r(t))$$
 (8)

$$S_{\pm 4}(t) = H_4(t) \int_{\infty}^{\infty} dr \, \exp(\pm i \, 2\pi \, 4 \, f_r(t) r) C_{2P}(r) = H_4(t) \tilde{C}_{2P}(\pm 4 \, f_r(t))$$
(9)

The signal equations can then be simply written for any value q, and only the positive portion of the Fourier Transform is needed. Additional considerations taken in the signal function include rotation rate and mounting error. The SPIFI mask will rotate at some temporal frequency ν_c and this effect needs to be included in the time signal. Another factor to consider is that if the mask is not perfectly mounted on the center of the rotation axis, the modulation frequencies will "wobble" throughout rotation. An example of this is shown in Figure 2. This wobble is analytically modelled as a phase term with time dependence $\phi(t)$. This phase term can be extracted by analysing the SPIFI carrier frequency throughout rotation with a stepped windowed Fourier Transform known as the Gabor Transform. Both the carrier frequency and the wobble also depend on the SPIFI order q, and the signal equation including these factors is shown in Equation 10.

$$S_q(t) = H_q(t) \operatorname{Re} \left[\exp(i \, 2\pi \, q \nu_c t) \exp(i \, q \, \phi(t)) \tilde{C}_{2P}(q \, f_r(t)) \right]$$
(10)

The result is a signal with multiple orders that yield increasing spatial frequency support. An additional consideration not yet mentioned for multiphoton microscopy is the pulse duration at the sample and dispersion

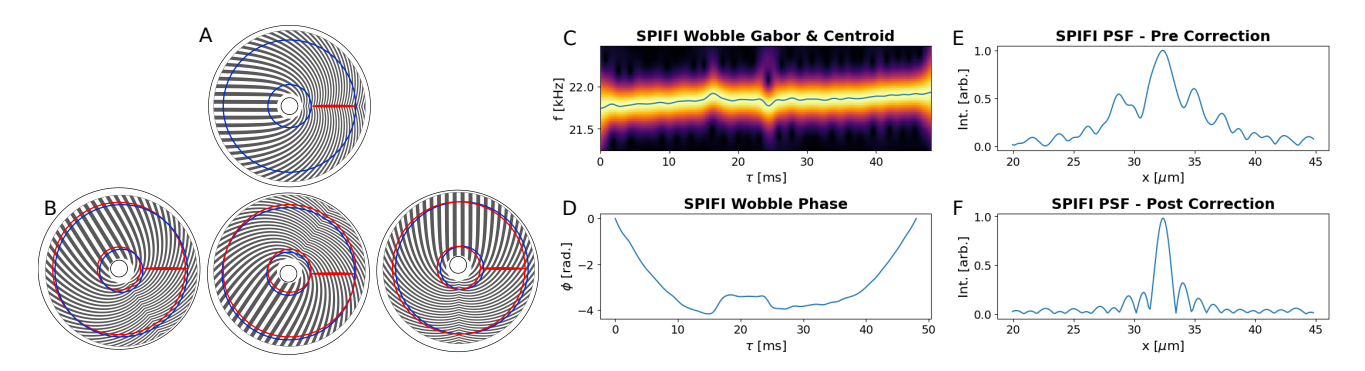


Figure 2. **A**: A perfectly centered mounted SPIFI mask corresponding to a wobble phase of $\phi(t) = 0$. The blue lines show that the leftmost and rightmost pixels along the line cursor maintain a constant radius from the center of the mask. **B**: An off-center mask at three rotation angles. The red circles show the varying radii from the true center of the mask, yielding a wobble phase. **C**: A Gabor Transform of 1st order SPIFI data showing the central modulation frequency shifting through time. The blue line is the centroid. **D**: The wobble phase obtained via a cumulative integral of the centroid in **C**. **E**: The PSF prior to wobble correction. **F**: The PSF following wobble correction.

inherent to the imaging system. As is apparent from the analysis in Equation 5, the higher order terms have significantly lower signal amplitudes. Temporal stretching of the laser pulse greatly reduces multiphoton signals and exponentially reduces the higher order signal amplitudes. Thus to obtain enhanced resolution from the higher orders, optimized dispersion compensation is necessary. Here we introduce a system which employs SPIFI in two domains to perform enhanced resolution nonlinear microscopy and compensate for second order dispersion with a rapid and facile method. Significantly, the presented dispersion compensation method accounts for second order dispersion all the way through to the sample plane, providing an in-line technique with no need to divert the beam to make a measurement independent of the microscope system.

2. OPTICAL SYSTEM

A Thorlabs Y-Fi HP source (λ_0 =1035 nm, $\Delta t \le 220$ fs, f=10 MHz) was used to test the cascaded WD-SD-SPIFI system. The WD-SPIFI subsystem was built in to a Martinez dispersion compensation system with two gratings (Lightsmyth T-1000-1040-31.8x24.8-94) at Littrow configuration and two lenses (Thorlabs AC508-100-B-ML) with all components initially in the 4f configuration. The WD-SPIFI system was built on a rail with carriers (Newport PRL-24 and PRC-3) for easy adjustment of the spacing of the second grating from the second lens. A SPIFI mask machined onto a glass disk using an in-house laser machining system²⁶ was mounted to a motor (Trinamic QSH2818). With the SPIFI pattern at f of the first lens the spectrum is diffracted variably with mask rotation as in SD-SPIFI. The varying diffraction in this system causes delayed, lower intensity copies of the pulse to sweep across each-other in time at the sample plane. The result is a cross-correlation signal which exhibits dependence on the pulse width. The second grating of the WD-SPIFI system can be shifted to add negative second order dispersion (Group Delay Dispersion - GDD) to compensate for positive second order dispersion due to glass downstream. WD-SPIFI allows for real-time optimization of this dispersion compensation all the way through the microscope into a nonlinear sample. The multiphoton signal is then captured and can be viewed on an oscilloscope and optimized by hand in real time. Example data from optimizing the GDD for the SD-SPIFI system is presented in Section 3.

The SD-SPIFI subsystem follows the WD-SPIFI subsystem and focuses the beam into a line cursor with a cylindrical lens (Thorlabs LJ1567L1-B) onto a SPIFI mask. The SPIFI mask was manufactured by InLight Gobo and was mounted onto a motor (Faulhaber Minimotor SA). The exposure time for a single line image without averaging was \sim 15 ms. Inconsistent motor speed is apparent and adjusts temporal modulation frequencies which blurs images from trace to trace. This is mitigated by monitoring a separate laser focused on the SPIFI mask. The signal from this timing laser enables consistent oscilloscope triggering and measuring of the duration between timing pulses on the SPIFI mask; this timing signal enables signal interpolation onto a common time grid. The modulation plane was imaged to the sample plane through a tube lens (Thorlabs TTL200MP) and

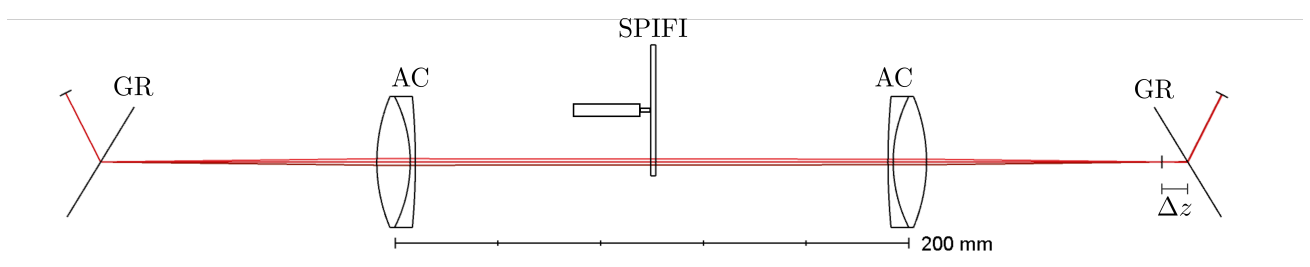


Figure 3. The Wavelength-Domain SPIFI system is a Martinez pulse compressor with a SPIFI mask at focus between the lenses. Offsetting the output grating past focus adds negative GDD. GR: grating; AC: achromat; SPIFI: SPIFI mask on motor.

microscope objective (Olympus UPLFLN 40x). A Collection Optic with High Numerical Aperture (COHNA²⁷) with built-in space for an interchangeable filter was placed after the sample to collect multiphoton signal light onto a Photomultipler Tube (PMT - Hammamatsu H7422P-40). The output signal is transmitted via double shielded SMA cable (Pasternack PE3M0034) to a transimpedance amplifier (Thorlabs TIA60) and measured with an oscilloscope terminated on 50 Ohms (Digilent Analog Discovery Pro ADP3450) using a custom Python script. This script handles acquisition as well as scan control, communicating serially with a motor controller and stepper motors (Newport ESP301 and Newport LTA-HS).

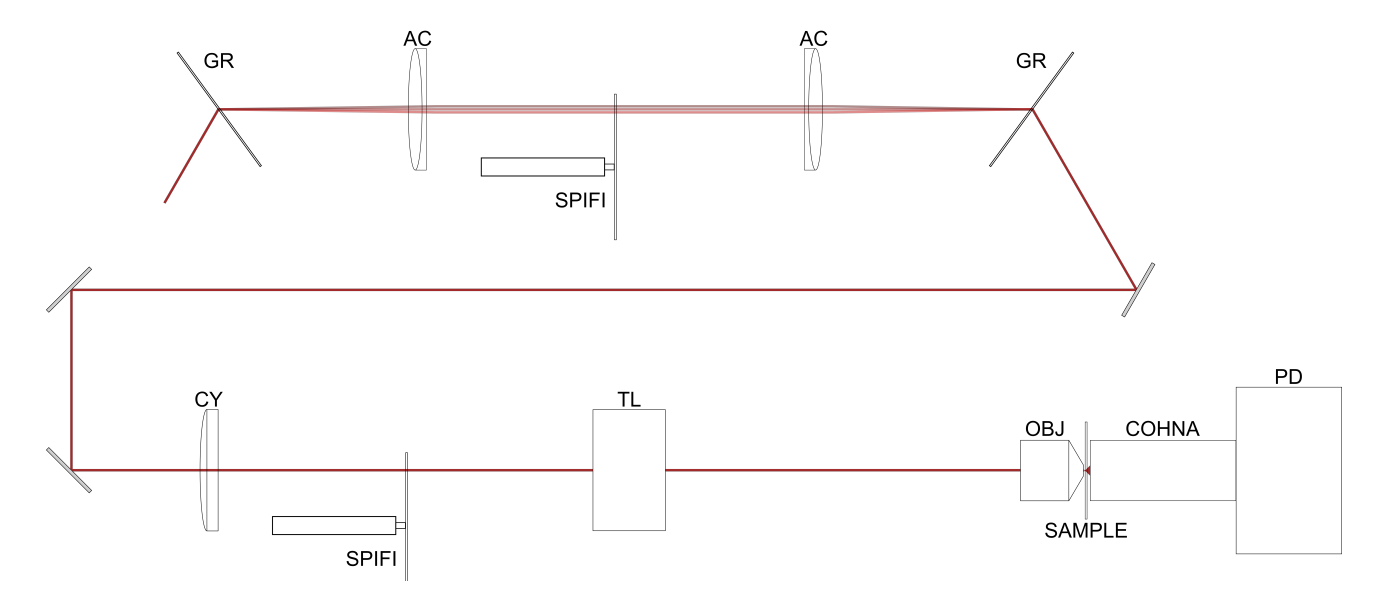


Figure 4. The SD-SPIFI subsystem directly follows the WD-SPIFI subsystem. The output grating offset is coupled with the following mirror such that GDD can be compensated without realignment. CY: cylindrical lens; TL: tube lens; OBJ: objective lens; COHNA: Collection Optic with High Numerical Aperture; PD: Photodetector (Photodiode or Photomultiplier tube).

3. RESULTS

The WD-SPIFI subsystem was used to optimize the dispersion compensation of the Martinez system by setting the position of the output grating according to the FWHM of the cross-correlated nonlinear signal generated by a TPEF dye at the focus of the microscope objective. Initially, this was done with another microscope objective (Zeiss A-Plan 40x). The output grating was scanned in steps of 1 mm starting from a distance of -7 mm from the zero dispersion position to +23 mm past the zero dispersion point. At each grating position a time trace over the full rotation of the WD-SPIFI mask was taken with 30 sample averages. The peaks of the traces were

used to draw an envelope and the FWHM of each was found. The results are shown in Figure 5 which shows an optimal point at the lowest FWHM of the WD-SPIFI trace at a grating offset of +10 mm. This point indicates the optimal dispersion compensation as it shows a correlation of the shortest pulses at focus. This result was compared against the full pulse characterization technique Dispersion Scan. ^{28–30} The Dispersion Scan was taken over the same grating positions and shows a peak intensity at the same grating position as was found by the WD-SPIFI optimization. Running the dispersion scan through its iterative phase retrieval algorithm showed a temporal pulse width of 209 fs and confirms the optimal location of the grating found in WD-SPIFI.

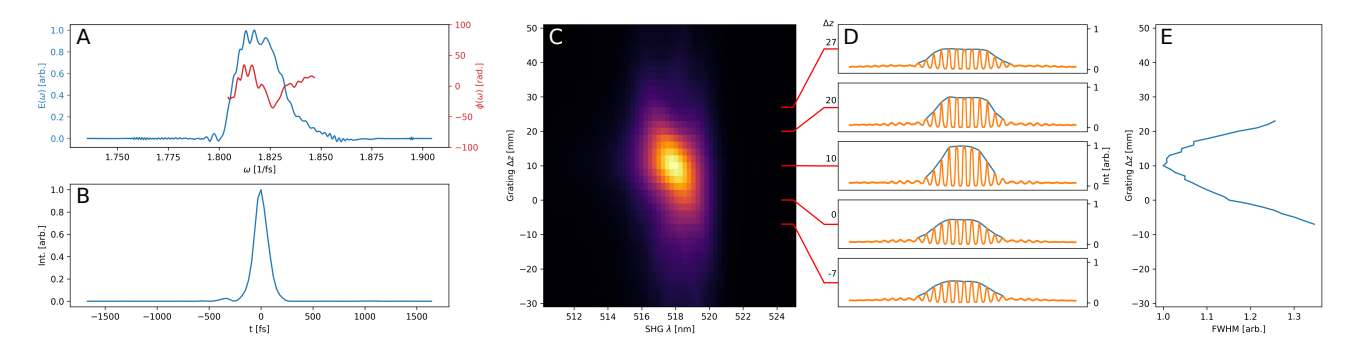


Figure 5. A: Spectral phase and amplitude retrieved from dispersion scan. B: temporal profile retrieved from Dispersion Scan. C: Dispersion Scan measurement showing spectral intensity at varying grating positions. D: WD-SPIFI traces with envelopes at grating positions corresponding to those in Dispersion Scan. E: FWHM of envelopes in WD-SPIFI as a function of grating position.

The WD-SPIFI optimization system allows for flexibility in the optical system without time-intensive recharacterization. For the following resolution results, the objective was changed back to the Olympus UPlan FLN 40x objective, the cylindrical lens was changed to a 50 mm achromatic cylindrical lens (ThorLabs ACY254-050-B), a beam expander prior to the SD-SPIFI system was removed, and the internal dispersion compensation of the Y-Fi laser was reduced to 0. With a quick GDD compensation recalibration using the WD-SPIFI system, the offset of the grating increased to +16 mm.

In the SD-SPIFI subsystem we show that resolution characterization is possible both by measuring the Point Spread Function (PSF) via imaging a sub-diffractive object, and also by measuring the Modulation Transfer Function (MTF) directly using the spatial frequencies of the mask imaged through the system.

Measuring the Point Spread Function is a common metric for system performance. The PSF was measured by imaging a sub-diffractive fluorescent nanodiamond. The 140 nm nanodiamond (Adamas Nano NDNV140nmMd) exhibits 2PEF under the 1035 nm pulsed laser. Because SPIFI images are generated in the temporal frequency domain, a calibration is required to determine the relationship between a pixel's blinking frequency on the mask and its position at focus. For this calibration a USAF target was placed at focus and light was collected onto a photodiode. The center-to-center distances of each bar of each element in group 6 were measured in frequency space and compared to their separation in space. This yielded a calibration of $1.32 \times 10^{-8} \ \mu\text{m}/\text{Hz}$ with an uncertainty of $\pm 2.54 \times 10^{-10} \ \mu\text{m}/\text{Hz}$. At the effective NA of 0.5, which was determined by measuring the ± 1 diffracted SPIFI order spread at the objective pupil plane, a diffraction-limited point-scanning system would be limited to a PSF FWHM of $1.056 \ \mu\text{m}$ according to $0.51\lambda/\text{NA}$. With SPIFI, we demonstrate a PSF FWHM of $1.46 \pm 0.03 \ \mu\text{m}$ in the first order and $0.78 \pm 0.01 \ \mu\text{m}$ in the second order, which beats the standard diffraction limit. The resolution measurement profiles are shown in Figure 6.

The MTF measurement was done by placing a two-photon excitation dye at the objective focus and imaging the fluorescence in the epi-direction off of a dichroic (Semrock LF635) onto a camera (AmScope MU1000). To accommodate the magnification and pixel size of the camera to avoid aliasing, this measurement was done with a large pupil objective to underfill to an effective NA of 0.12. This low NA kept spatial frequencies within a measurable range on this camera. Images of the modulated line cursor were taken at multiple rotation steps. The line profile at each step was analyzed to measure transmitted intensity as well as spatial frequency. The spatial frequency grid at focus was calibrated to the camera image by imaging a dyed USAF 1951 Resolution

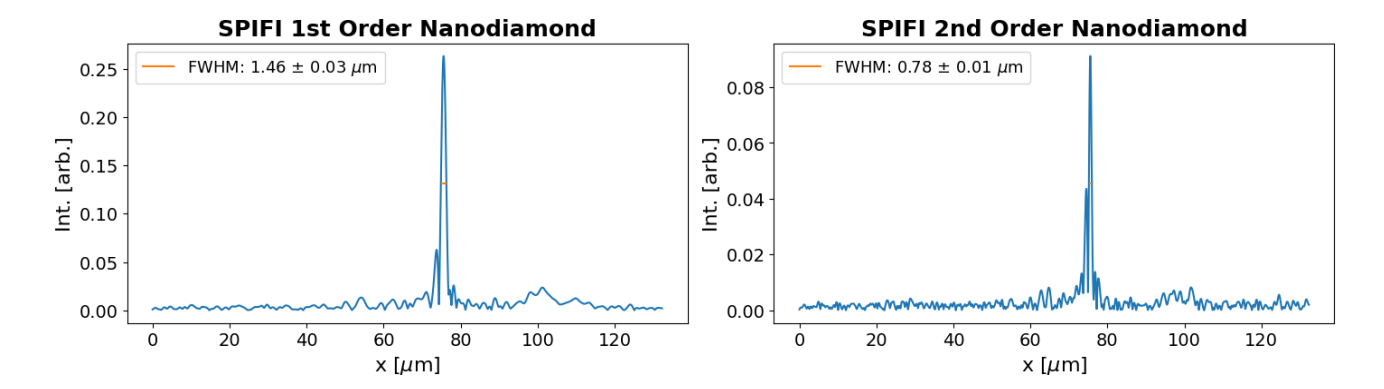


Figure 6. SPIFI axis profile images of sub-diffractive fluorescent nanodiamond in 2PEF. The 1st and 2nd orders are shown with their PSF FWHM values. The 2nd order FWHM is lower than the classical limit for this wavelength.

Test Target to the camera and measuring bar widths in pixels. The measured MTF showing relative intensity as a function of spatial frequency is shown in Figure 7. The shape of the MTF matches that of Figure 5 from the analysis done in 25. Here the spatial frequency is limited by the mask itself, not the imaging system. If the mask had higher spatial frequencies the intensity rollover would be expected to continue down to zero at the cutoff frequency.

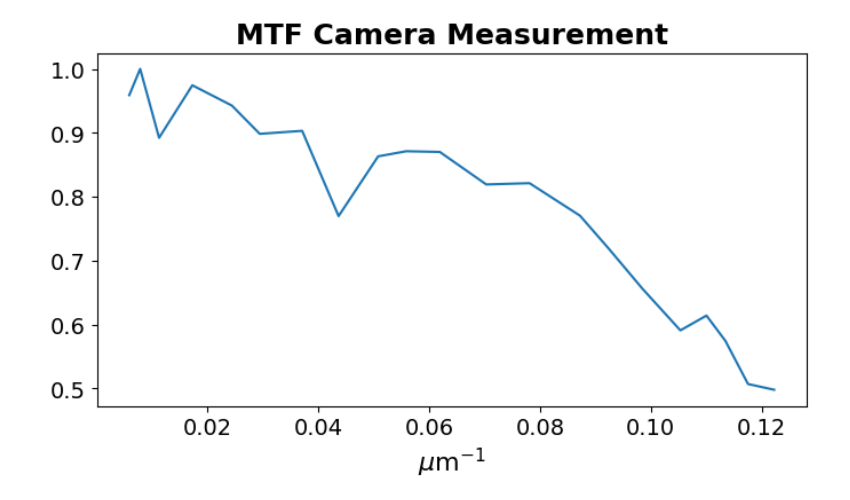


Figure 7. Measured modulation transfer function of the SPIFI system. Shape of decay corresponds to prior SPIFI MTF analysis in 25.

SPIFI is also compatible with harmonic generation. A Bismuth Halide sample was imaged with both Second Harmonic Generation (SHG) and Third Harmonic Generation (THG). In both of these modalities, the improvement in resolution in the second order is apparent. Along one line capture on the SPIFI axis, marked in red in Figures 8 and 9, the comparison between 1st and second order shows significantly more detail and discernment in features. There is however lower SNR due to the lower amplitude of the higher order SPIFI signals.

4. NEXT STEPS

All image results presented here are from signals acquired on an oscilloscope with the only post processing being of wobble correction, timing alignment, and FFT averaging. These analog signals from a PMT can be significantly improved with a digitized photon counting approach. Using a threshold to increment counts in discrete time bins that correspond with incident excitation pulses reduces extraneous noise and builds up a signal over time which

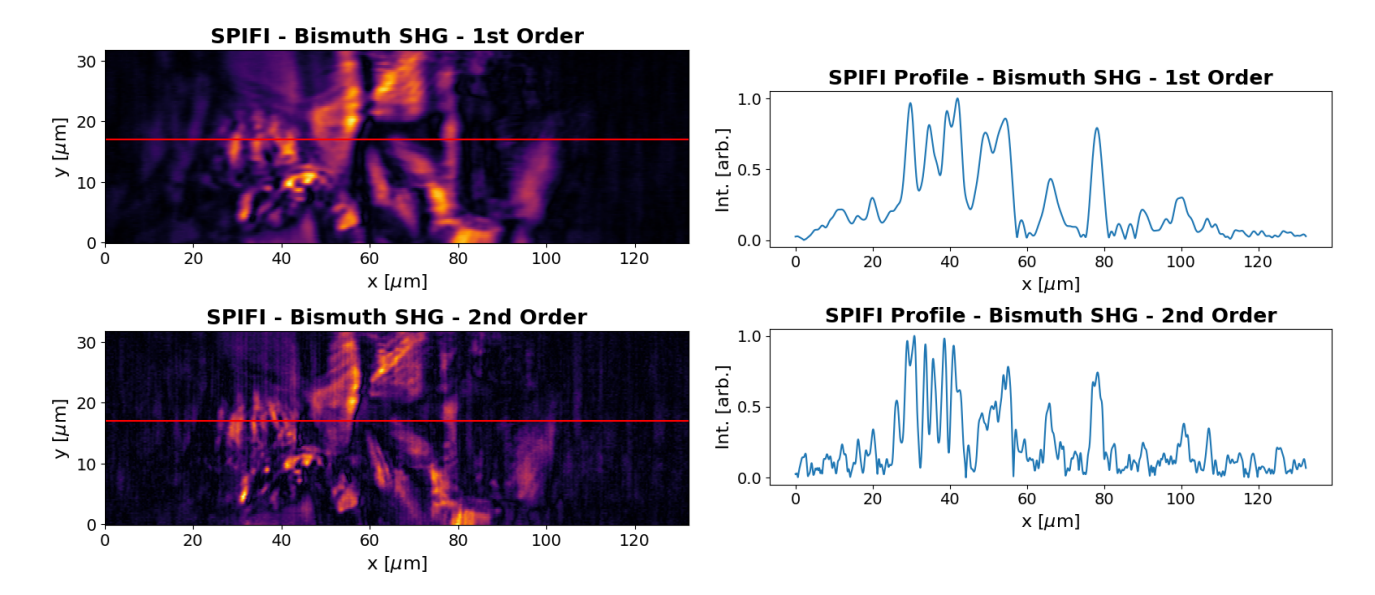


Figure 8. Second Harmonic Generation (SHG) signal of a bismuth halide sample in the 1st and 2nd SPIFI orders. Line profile from the red lines are shown to emphasize the resolution enhancement in the 2nd order.

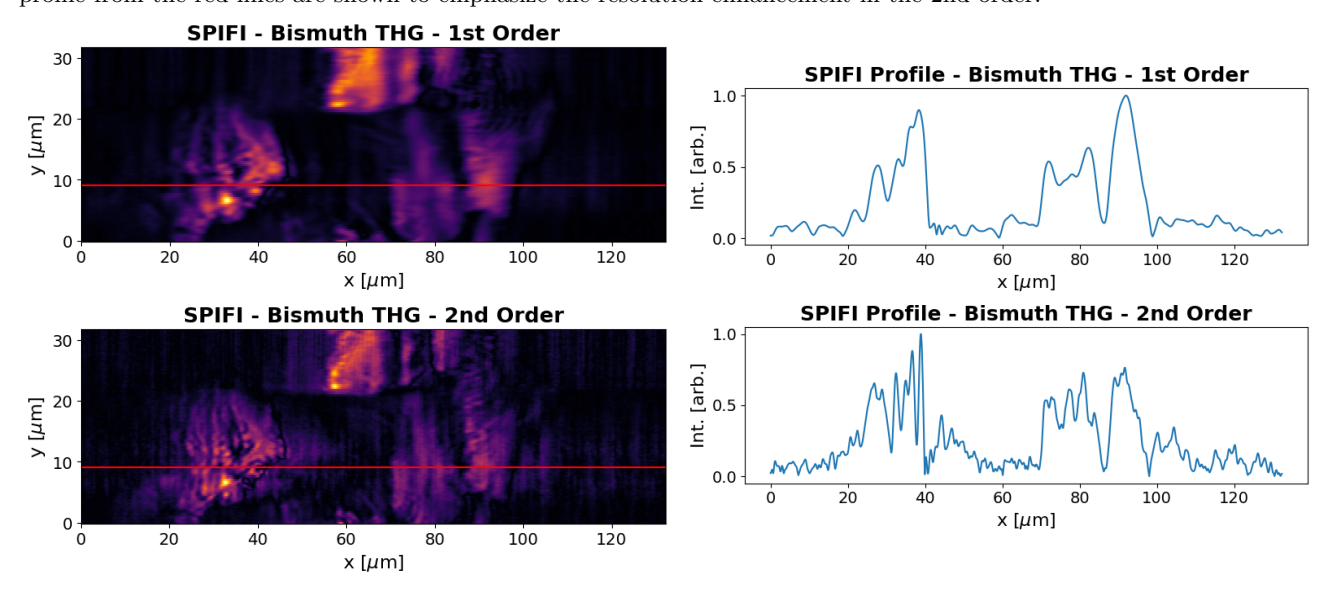


Figure 9. Third Harmonic Generation (THG) signal of a bismuth halide sample in 1st and 2nd SPIFI orders. Line profile from the red lines are shown to emphasize the resolution enhancement in the 2nd order.

reduces SNR and enables higher exposure times. This improvement in SNR will make 3rd and 4th order imaging more reliable to potentially get nearly a 4X resolution enhancement. Currently, 3rd and 4th order images are obtained but due to noise the resolution results are not repeatable enough to report.

5. CONCLUSION

We have presented a cascaded SPIFI system that modulates in both the wavelength domain and the spatial domain. By modulating only the wavelength domain, second order dispersion compensation is optimized through the full imaging system by moving a translation stage and viewing a real-time signal. This result has been

confirmed with a full pulse characterization technique, Dispersion Scan, and the WD-SPIFI optimization is readily and quickly repeated following any system changes.

With the spatial domain SPIFI system, we have demonstrated enhanced resolution in multiple multiphoton modalities (2PEF, SHG, THG) with a PMT and no photon counting or post-processing beyond averaging and standard SPIFI image generation. The MTF of the system was also measured through the objective and aligns with expectations from theoretical analysis of SPIFI.

ACKNOWLEDGMENTS

We would like to thank the National Science Foundation (NSF) for their support (Grant No. 1707287).

Open source Python libraries were essential to the work presented here. The authors would like to recognize the efforts of everyone who has contributed to NumPy,³¹ SciPy,³² and Matplotlib.³³

REFERENCES

- [1] Köhler, A., "New method of illumination for photomicrographical purposes," *Journal of the Royal Microscopical Society* **14**, 261–262 (1894).
- [2] Lim, D., Chu, K. K., and Mertz, J., "Wide-field fluorescence sectioning with hybrid speckle and uniform-illumination microscopy," *Optics Letters* **33**, 1819 (Aug. 2008).
- [3] Santos, S., Chu, K. K., Lim, D., Bozinovic, N., Ford, T. N., Hourtoule, C., Bartoo, A. C., Singh, S. K., and Mertz, J., "Optically sectioned fluorescence endomicroscopy with hybrid-illumination imaging through a flexible fiber bundle," *Journal of Biomedical Optics* 14(3), 030502 (2009).
- [4] Mertz, J. and Kim, J., "Scanning light-sheet microscopy in the whole mouse brain with HiLo background rejection," *Journal of Biomedical Optics* **15**(1), 016027 (2010).
- [5] Choi, H., Yew, E. Y. S., Hallacoglu, B., Fantini, S., Sheppard, C. J. R., and So, P. T. C., "Improvement of axial resolution and contrast in temporally focused widefield two-photon microscopy with structured light illumination," *Biomedical Optics Express* 4, 995 (July 2013).
- [6] Xue, Y., Berry, K. P., Boivin, J. R., Wadduwage, D., Nedivi, E., and So, P. T. C., "Scattering reduction by structured light illumination in line-scanning temporal focusing microscopy," *Biomedical Optics Express* 9, 5654 (Nov. 2018).
- [7] Isobe, K., Takeda, T., Mochizuki, K., Song, Q., Suda, A., Kannari, F., Kawano, H., Kumagai, A., Miyawaki, A., and Midorikawa, K., "Enhancement of lateral resolution and optical sectioning capability of two-photon fluorescence microscopy by combining temporal-focusing with structured illumination," *Biomedical Optics Express* 4, 2396 (Nov. 2013).
- [8] Yeh, C.-H. and Chen, S.-Y., "Resolution enhancement of two-photon microscopy via intensity-modulated laser scanning structured illumination," *Applied Optics* **54**, 2309 (Mar. 2015).
- [9] Hinsdale, T. A., Stallinga, S., and Rieger, B., "High-speed multicolor structured illumination microscopy using a hexagonal single mode fiber array," *Biomedical Optics Express* 12, 1181 (Feb. 2021).
- [10] Hu, C., Wu, Z., Yang, X., Zhao, W., Ma, C., Chen, M., Xi, P., and Chen, H., "MUTE-SIM: multiphoton up-conversion time-encoded structured illumination microscopy," *OSA Continuum* 3, 594 (Mar. 2020).
- [11] Jin, L., Liu, B., Zhao, F., Hahn, S., Dong, B., Song, R., Elston, T. C., Xu, Y., and Hahn, K. M., "Deep learning enables structured illumination microscopy with low light levels and enhanced speed," *Nature Communications* 11, 1934 (Dec. 2020).
- [12] Wang, G., Zhao, F., Xiao, D., Shao, L., Zhou, Y., Yu, F., Wang, W., Liu, H., Wang, C., Min, R., Yan, Z., and Shum, P. P., "Highly efficient single-pixel imaging system based on the STEAM structure," *Optics Express* 29, 43203 (Dec. 2021).
- [13] Kanno, H., Mikami, H., and Goda, K., "High-speed single-pixel imaging by frequency-time-division multiplexing," *Optics Letters* **45**, 2339 (Apr. 2020).
- [14] Wijesinghe, P., Escobet-Montalbán, A., Chen, M., Munro, P. R. T., and Dholakia, K., "Optimal compressive multiphoton imaging at depth using single-pixel detection," *Optics Letters* 44, 4981 (Oct. 2019).
- [15] Hahamovich, E., Monin, S., Hazan, Y., and Rosenthal, A., "Single pixel imaging at megahertz switching rates via cyclic Hadamard masks," *Nature Communications* **12**, 4516 (Dec. 2021).

- [16] Donald J. Lovell, "Electro-optical position indicator system," (1961).
- [17] Driggers, R. G., Halford, C. E., Boreman, G. D., Lattman, D., and Williams, K. F., "Parameters of spinning FM reticles," *Applied Optics* **30**, 887 (Mar. 1991).
- [18] Futia, G., Schlup, P., Winters, D. G., and Bartels, R. A., "Spatially-chirped modulation imaging of absorbtion and fluorescent objects on single-element optical detector," *Optics Express* **19**, 1626 (Jan. 2011).
- [19] Howard, S. S., Straub, A., Horton, N. G., Kobat, D., and Xu, C., "Frequency-multiplexed in vivo multiplexed in photon phosphorescence lifetime microscopy," *Nature Photonics* 7, 33–37 (Jan. 2013).
- [20] Diebold, E. D., Buckley, B. W., Gossett, D. R., and Jalali, B., "Digitally synthesized beat frequency multiplexing for sub-millisecond fluorescence microscopy," *Nature Photonics* 7, 806–810 (Oct. 2013).
- [21] Hoover, E. E., Field, J. J., Winters, D. G., Young, M. D., Chandler, E. V., Speirs, J. C., Lapenna, J. T., Kim, S. M., Ding, S.-y., Bartels, R. A., Wang, J. W., and Squier, J. A., "Eliminating the scattering ambiguity in multifocal, multimodal, multiphoton imaging systems," *Journal of Biophotonics* 5, 425–436 (May 2012).
- [22] Worts, N., Czerski, J., Jones, J., Field, J. J., Bartels, R., and Squier, J., "Simultaneous multi-dimensional spatial frequency modulation imaging," *International Journal of Optomechatronics* 14, 1–17 (Jan. 2020).
- [23] Allende Motz, A. M., Czerski, J., Adams, D. E., Durfee, C., Bartels, R., Field, J., Hoy, C. L., and Squier, J., "Two-dimensional random access multiphoton spatial frequency modulated imaging," *Optics Express* 28, 405 (Jan. 2020).
- [24] Heuke, S., Sivankutty, S., Scotte, C., Stockton, P., Bartels, R. A., Sentenac, A., and Rigneault, H., "Spatial frequency modulated imaging in coherent anti-Stokes Raman microscopy," *Optica* 7, 417 (May 2020).
- [25] Field, J. J., Wernsing, K. A., Domingue, S. R., Allende Motz, A. M., DeLuca, K. F., Levi, D. H., DeLuca, J. G., Young, M. D., Squier, J. A., and Bartels, R. A., "Superresolved multiphoton microscopy with spatial frequency-modulated imaging," *Proceedings of the National Academy of Sciences* 113, 6605–6610 (June 2016).
- [26] Worts, N., Young, M., Field, J., Bartels, R., Jones, J., and Squier, J., "Fabrication and characterization of modulation masks for multimodal spatial frequency modulated microscopy," *Applied Optics* 57, 4683 (June 2018).
- [27] Young, M. D., Field, J. J., Sheetz, K. E., Bartels, R. A., and Squier, J., "A pragmatic guide to multiphoton microscope design," *Advances in Optics and Photonics* 7, 276 (June 2015).
- [28] Miranda, M., Fordell, T., Arnold, C., L'Huillier, A., and Crespo, H., "Simultaneous compression and characterization of ultrashort laser pulses using chirped mirrors and glass wedges," *Optics Express* **20**, 688 (Jan. 2012).
- [29] Loriot, V., Gitzinger, G., and Forget, N., "Self-referenced characterization of femtosecond laser pulses by chirp scan," *Optics Express* **21**, 24879 (Oct. 2013).
- [30] Wilhelm, A. M., Schmidt, D. D., Adams, D. E., and Durfee, C. G., "Multi-mode root preserving ptychographic phase retrieval algorithm for dispersion scan," *Optics Express* **29**, 22080 (July 2021).
- [31] Harris, C. R., Millman, K. J., van der Walt, S. J., Gommers, R., Virtanen, P., Cournapeau, D., Wieser, E., Taylor, J., Berg, S., Smith, N. J., Kern, R., Picus, M., Hoyer, S., van Kerkwijk, M. H., Brett, M., Haldane, A., del Río, J. F., Wiebe, M., Peterson, P., Gérard-Marchant, P., Sheppard, K., Reddy, T., Weckesser, W., Abbasi, H., Gohlke, C., and Oliphant, T. E., "Array programming with NumPy," Nature 585, 357–362 (Sept. 2020).
- [32] Virtanen, P., Gommers, R., Oliphant, T. E., Haberland, M., Reddy, T., Cournapeau, D., Burovski, E., Peterson, P., Weckesser, W., Bright, J., van der Walt, S. J., Brett, M., Wilson, J., Millman, K. J., Mayorov, N., Nelson, A. R. J., Jones, E., Kern, R., Larson, E., Carey, C. J., Polat, Feng, Y., Moore, E. W., VanderPlas, J., Laxalde, D., Perktold, J., Cimrman, R., Henriksen, I., Quintero, E. A., Harris, C. R., Archibald, A. M., Ribeiro, A. H., Pedregosa, F., van Mulbregt, P., SciPy 1.0 Contributors, Vijaykumar, A., Bardelli, A. P., Rothberg, A., Hilboll, A., Kloeckner, A., Scopatz, A., Lee, A., Rokem, A., Woods, C. N., Fulton, C., Masson, C., Häggström, C., Fitzgerald, C., Nicholson, D. A., Hagen, D. R., Pasechnik, D. V., Olivetti, E., Martin, E., Wieser, E., Silva, F., Lenders, F., Wilhelm, F., Young, G., Price, G. A., Ingold, G.-L., Allen, G. E., Lee, G. R., Audren, H., Probst, I., Dietrich, J. P., Silterra, J., Webber, J. T., Slavič, J., Nothman, J., Buchner, J., Kulick, J., Schönberger, J. L., de Miranda Cardoso, J. V., Reimer, J., Harrington, J., Rodríguez, J. L. C., Nunez-Iglesias, J., Kuczynski, J., Tritz, K., Thoma, M., Newville, M.,

Kümmerer, M., Bolingbroke, M., Tartre, M., Pak, M., Smith, N. J., Nowaczyk, N., Shebanov, N., Pavlyk, O., Brodtkorb, P. A., Lee, P., McGibbon, R. T., Feldbauer, R., Lewis, S., Tygier, S., Sievert, S., Vigna, S., Peterson, S., More, S., Pudlik, T., Oshima, T., Pingel, T. J., Robitaille, T. P., Spura, T., Jones, T. R., Cera, T., Leslie, T., Zito, T., Krauss, T., Upadhyay, U., Halchenko, Y. O., and Vázquez-Baeza, Y., "SciPy 1.0: fundamental algorithms for scientific computing in Python," *Nature Methods* 17, 261–272 (Mar. 2020).

[33] Hunter, J. D., "Matplotlib: A 2D Graphics Environment," Computing in Science & Engineering 9(3), 90–95 (2007).